Measurement 171 (2021) 108763

Contents lists available at ScienceDirect

Measurement

journal homepage: www.elsevier.com/locate/measurement

Surface monitoring of road pavements using mobile crowdsensing technology

Francesco Abbondati [a], Salvatore Antonio Biancardo [b,*], Rosa Veropalumbo [b], Gianluca Dell'Acqua [b]

[a] Department of Engineering, University of Naples Parthenope, Naples 80143, Italy
[b] Department of Civil, Construction, and Environmental Engineering (DICEA), University of Naples Federico II, Naples 80125, Italy

ARTICLE INFO

Keywords:
Continuous monitoring
Crowdsensing technology
Pavement distress
Punctual surveys
Road surface

ABSTRACT

Pavement-surface characteristics should be considered during road maintenance for safe and comfortable driving. A detailed and up-to-date report of road-pavement network conditions is required to optimize a maintenance plan. However, manual road inspection methods, such as periodic visual surveys, are time-consuming and expensive. A common technology used to address this issue is SmartRoadSense, a collaborative system for the automatic detection of road-surface characteristics using Global Positioning System receivers and triaxial accelerometers contained in mobile devices. In this study, the results of the SmartRoadSense surveys conducted on Provincial Road 2 (SP2) in Salerno, Italy, were compared with the Distress Cadastre data for the same province and the pavement condition indices of different sections of the SP2. Although the effectiveness of the crowdsensing-based SmartRoadSense was found to vary with the distress type, the system was confirmed to be very efficient for monitoring the most critical road failures.

1. Introduction

Since the late 1950s, several studies have demonstrated the influence of road-pavement surface conditions on driving safety and comfort. However, maintenance of such surfaces involves both direct costs (i.e., infrastructure maintenance) and indirect costs (i.e., services). Conversely, poorly maintained roads increase the fuel consumption and emissions of vehicles and adversely affect their suspension systems [1] and other mechanical components [2-4]. Different methods and technologies have recently been developed for the accurate measurement of road-surface characteristics, such as 3D texture morphologies [5] and smartphone-based near-infrared (NIR) molecular sensors [6], with the latter affording advanced characterization of asphalt concrete.

Various studies have also been conducted for the automatic detection of specific road anomalies. For example, Wong [7] modeled the vertical profile of a road surface using impulsive functions, triangular waves, and sinusoidal signals. Gillespie [8] also modeled the vertical profiles of a road surfaces as sums of randomly generated sinusoidal signals and showed that the spectral power density of a road surface had a low-pass characteristic that decreased with increasing spatial frequency. Other stochastic models having low-pass characteristics have been used to describe the randomness of road profiles measured by non-homogeneous Gaussian processes [9].

Studies have also been conducted on the use of autonomous accelerometers and accelerometers incorporated in mobile devices for the detection and georeferencing of bumps, potholes, and other isolated road-surface anomalies. For example, an independent accelerometer was used to assess road surface conditions in a prior study [10]. Eriksson et al. [11] used one with a sampling frequency of 380 Hz (higher than the ones found in most current mobile devices) to detect potholes and bumps from moving vehicles. Some components of the latest models of mobile communication devices, such as accelerometers, microphones, Global System for Mobile communications radios, and Global Positioning System (GPS) receivers, have also been used to analyze road-surface conditions and traffic [12]. Data acquired by smartphone sensors have likewise been used to detect potholes, bumps, vehicle braking, and horn sounds. Chen et al. [13] proposed a crowdsourcing-based surface monitoring system that could detect potholes and assess road roughness by means of temporary hardware installed on 100 taxi vehicles in Shenzhen. A Gaussian mixture model was used to evaluate the international roughness index (IRI) via statistical calculation.

Yi et al. [14] used mobile-device accelerometers to investigate road

* Corresponding author.
E-mail address: salvatoreantonio.biancardo@unina.it (S.A. Biancardo).

https://doi.org/10.1016/j.measurement.2020.108763
Received 3 August 2020; Received in revised form 14 November 2020; Accepted 18 November 2020
Available online 24 November 2020

anomalies, classifying them as artificial deceleration bumps, manholes, and deceleration stripe potholes. The vertical component of acceleration was calculated by averaging the acceleration caused by gravity. The oscillations of this vertical component of acceleration, caused by anomalies, were modeled using an oscillatory system without damping. The events were determined by comparing the vertical component of the acceleration with its normal standard deviation.

In some recent studies [15-18], data acquired by mobile-device accelerometers were used to formulate a roughness index for characterizing the conditions of a road surface. The SmartRoadSense system [18] has been in use since 2013, and it is currently active in Italy, the UK, Romania, Greece, and Portugal. An outline of the system is provided as follows:

- Mathematical models based on predictive algorithms are used to process data acquired by an accelerometer with GPS.
- A mobile-resident application transmits the road-roughness data to a central server.
- A server-side application receives, aggregates, and periodically updates the incoming data.
- Numerical data are released in an open format for road mapping and easy viewing.

The accelerometer data are divided into 1-s windows, and, for each, a linear predictive coding (LPC) analysis is conducted on the signals to remove all predictable components. The signal components that vary slowly or periodically include acceleration caused by gravity, vehicle acceleration, centrifugal acceleration, rolling, pitching, yawing, and engine vibrations. The *prediction residue* of the LPC analysis retains the unpredictable acceleration components, which are mostly associated with the effects of the road surface on vehicle tires and suspension. The *power of the prediction residue* is then determined and used to estimate the road roughness index. The GPS coordinates, vehicle speed, and determined road roughness index are periodically transmitted to a remote data server. The data acquired from different mobile devices are aggregated with consideration of their different sensitivities [19]. The overall data are then stored in a geographical information system (GIS) that maps the weighted-average data for a given road.

The SmartRoadSense application became fully operational on February 21, 2015. By December 31, 2015, it had covered 24,664.4 km (5.06%) of the Italian road network. The application database currently contains>3,000,000 road roughness indices.

In a study conducted after the rollout of SmartRoadSense [20], an independent accelerometer connected to a laptop was used to acquire data, which was then analyzed in a laboratory. The analysis was largely based on the *power of vertical acceleration*, as proposed by Alessandroni et al. [18]. In another recent study [21], the unevenness of an unpaved road was evaluated based on the power spectral density (PSD) of the road-surface profile as measured by a stereoscopic camera.

The pavement condition index (PCI) is used to quantify the pavement conditions of roads and parking lots through visual inspection. It was developed by the U.S. Army Corps of Engineers [22,23] as a numerical indicator of the surface condition of asphalt and concrete pavements with a value range of 0–100. The PCI does not reflect structural capacity, nor does it provide direct indications of skid resistance and roughness. However, it affords an objective basis for determining maintenance and repair requirements and priorities. Many studies on PCI and its application have been conducted. For example, Sharaf et al. [24] presented a procedure for determining the best maintenance and repair alternatives at the road-network level and related costs for different pavement categories and PCI ranges. Shahnazari et al. [25] also developed an alternative approach for forecasting PCI using optimization techniques that included artificial neural networks and genetic programming. In [26], an overall PCI (OPCI) for urban road networks was presented. Four individual performance indices were defined (i.e., distress index ($PCI_{Distress}$), roughness index ($PCI_{Roughness}$), structural-capacity index ($PCI_{Structure}$), and skid-resistance index (PCI_{Skid})), which were combined to derive the OPCI.

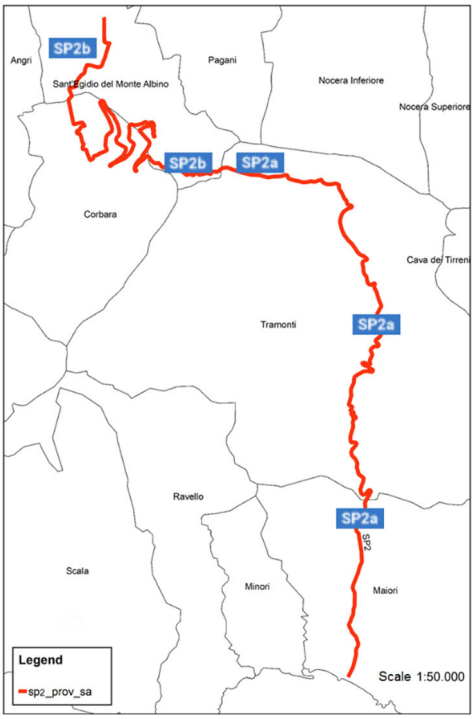

Fig. 1. Highway SP2.

In addition to existing consolidated technical methods, some Italian administrations have developed their own registers of pavement road deterioration that use subjective discriminations of types and intensities of distress based on visual inspection with manual thickness and length measurements.

The purpose of the present study is to evaluate the effectiveness of recent mobile technologies for detecting different types of road pavement-surface distresses. Open data available on the crowdsensing-based SmartRoadSense system are compared with the results of two visual methods. The reference field is the asphalt–concrete pavement of Provincial Road 2 (SP2) in Salerno, Italy. The first comparison uses data recorded in the Distress Cadastre of the Province of Salerno. This Cadastre is a subjective registry established by the administrators of the Province. The second comparison uses the PCIs of SP2 sections as recorded by the present authors. Specifically, SmartRoadSense provides a roughness index more comparable to other surface characteristics indices (e.g., friction, IRI, and macro-/micro-textures) used in the practice of road-pavement analysis, whereas Cadastre and the PCI method provide global status indices. Comparisons are then made between the SmartRoadSense index and the Cadastre + PCI indices. The objective is to determine whether any of the currently used advanced monitoring technologies, known to be economically attractive, can be effectively used to replace visual road inspections for the detection of all types of pavement-surface distresses.

2. Materials and methods

Highway SP2 in Salerno, Italy is the focus of this study. The highway extends over 21.6 km, connecting highway SP3 with highway SS163 (Fig. 1). It is divided into two branches: SP2a (11.6 km) and SP2b (10.0 km).

Previous studies have reported the poor asphalt maintenance of the SP2. There are widespread distresses in the upper surface layer, including cracking, patching, potholes, rutting, and raveling. The underlying layers also contain distresses, such as depressions, bumps, and

sags [27].

2.1. Data collection and SmartRoadSense data

The sensitivity and sampling frequencies of current smartphone accelerometers are about 100–300 Hz, which enable the detection of vibrations transmitted from the road superstructure to a vehicle. Each mobile device connected to the SmartRoadSense system is mounted on a rigid support inside a car. Analysis of the signals acquired by the accelerometer and GPS navigator enables the location and classification of road-surface anomalies that cause various types of vibrations. The computing and communication power of current mobile devices facilitate real-time processing of the acquired data within the device itself. During processing, the condition of the road surface is described using a roughness index, and the georeferenced data is transmitted to a server. The roughness values are then averaged and weighted over time and space, stored in a GIS, and released in an open format.

The SmartRoadSense mobile application leverages the power of the prediction residue of an autoregressive model. Basically, when the road surface is uniform, the accelerations detected by the mobile device are of the same nature and are predictable. The power of the prediction residue increases with increasing surface roughness, and when an anomaly is encountered on the road, the power of the prediction residue increases. The average power is used to estimate the road roughness index.

Gillespie [8] showed that the typical PSD of the vertical profile of a road surface had a low-pass characteristic that decreased with increasing spatial frequency. Hence, the road surface could be described using white Gaussian noise (WGN) filtered through a first-order low-pass filter. In the frequency domain, the WGN is a constant determined by the power of the noise itself. The first-order low-pass filter introduces a pole. The statistical properties of the road surface are determined from the spectral power of the WGN and the pole of the low-pass filter. The PSD of the vertical profile of the road surface in the spatial domain, $S_{rr}(j\Lambda)$, is given by

$$S_{rr}(j\Lambda) = S_{ww}(j\Lambda)|H(j\Lambda)|^2 = q\left|\frac{1}{p+j\Lambda}\right|^2 \tag{1}$$

where $S_{ww}(j\Lambda) = \int_{-\infty}^{+\infty} q\delta(\Lambda)e^{-j\Lambda}d\Lambda = q$is the PSD of the autocorrelation function of the WGN, expressed as $\rho_{ww} = q\delta(\Lambda)$, q is the amplitude of the PSD, $\delta(\Lambda)$ is the delta function of Dirac, Λ is the spatial pulsation in radians per meter, and $H(j\Lambda) = \frac{1}{p+j\Lambda}$ is the first-order low-pass filter with pole p.

The properties of the vertical profile of the road surface can be fully statistically characterized when the parameters, q and p, are known. The PSD of the vertical profile in the time domain, $S_{rr}(j\Omega)$, can be expressed as

$$S_{rr}(j\Omega) = S_{ww}(j\Omega)|H(j\Omega)|^2 = q\left|\frac{1}{p+\frac{j\Omega}{v}}\right|^2 = S_{rr}\left(\frac{j\Lambda}{v}\right) \tag{2}$$

where Ω is the angular frequency in radians per second, and v is the vehicle speed [7]. The PSD of the vertical acceleration of a material point that travels along the vertical profile of a road surface at a constant speed, v [18], is given by

$$S_{A_yA_y}(j\Omega) = S_{ww}(j\Omega)\left|\frac{(j\Omega)^2}{p+\frac{j\Omega}{v}}\right|^2 = q\left|v\frac{(j\Omega)^2}{pv+j\Omega}\right|^2 \tag{3}$$

When the material point matches an anomaly on the road surface, the power of the prediction residue of the vertical acceleration increases. However, the acceleration perceived by the mobile device inside the vehicle is not equal to that at the tire–pavement interface. The latter is filtered by the mechanical couplings between the tires and suspensions of the vehicle before reaching the mobile device. The objective is to relate the power detected by the accelerometer of the mobile device with the acceleration at the tire–pavement interface. This can be achieved by balancing the forces according to the quarter-car model [28,29] for a single suspension:

$$\begin{bmatrix} M \\ m \end{bmatrix}\begin{bmatrix} \ddot{Z} \\ \ddot{Z}_u \end{bmatrix} + \begin{bmatrix} C_s & -C_s \\ -C_s & C_s \end{bmatrix}\begin{bmatrix} \dot{Z} \\ \dot{Z}_u \end{bmatrix} + \begin{bmatrix} K_s & -K_s \\ -K_s & K_s+K_t \end{bmatrix}\begin{bmatrix} Z \\ Z_u \end{bmatrix} = \begin{bmatrix} 0 \\ K_tZ_r \end{bmatrix} \tag{4}$$

where M is the sprung mass, m is the unsprung mass, Z is the displacement of the sprung mass, Z_u is the displacement of the unsprung mass, Z_r is the displacement of the road surface, C_s is the suspension damping constant, K_s is the suspension stiffness, K_t is the tire stiffness, and $\dot{Z}$, $\dot{Z}_u$, $\ddot{Z}$, and $\ddot{Z}_u$ are respectively the first and second derivatives of the sprung and unsprung mass displacements with respect to time. The transfer function between the acceleration at the tire–pavement interface and the residual acceleration inside the vehicle, $\ddot{Z}/\ddot{Z}_r$, in the frequency domain is

$$\frac{\ddot{Z}(j\Omega)}{\ddot{Z}_r(j\Omega)} = \frac{Dj\Omega+1}{A(j\Omega)^4 + B(j\Omega)^3 + C(j\Omega)^2 + Dj\Omega + 1} \tag{5}$$

where

$$A = \frac{\chi}{K_1K_2}(\sec^4); B = c\frac{1+\chi}{K_1K_2}(\sec^3); C = \frac{K_1+\chi K_2+K_2}{K_1K_2}(\sec^2); D = \frac{c}{K_2}(\sec); \chi = \frac{m}{M}; c = \frac{C_s}{M}(1/\sec); K_1 = \frac{K_t}{M}(1/\sec^2); K_2 = \frac{K_s}{M}(1/s^2)$$

Several values of K_s, K_c, C_s, M, and m have been suggested [8,30-35] for the determination of A, B, C, and D and the calculation of the frequency response, $\frac{\ddot{Z}(j\Omega)}{\ddot{Z}_r(j\Omega)}$, of the quarter car model of Eq. (4).

Finally, the power of vertical acceleration measured by the accelerometer placed inside the vehicle [18] is given by

$$P(v) = \frac{1}{2\pi}\int_{-\infty}^{+\infty} S_{A_yA_y}(j\Omega)|S(j\Omega)|^2 d\Omega \tag{6}$$

where $S_{AyAy}(j\Omega)$ is the PSD of the vertical acceleration measured on the road surface, calculated using Eq. (3), which depends on the speed, v. $S(j\Omega)$ is the frequency response of the suspensions given by Eq. (4). In its expanded form,

$$P(v) = \frac{1}{2\pi}\int_{-\infty}^{+\infty} q\left|v\frac{(j\Omega)^2}{pv+j\Omega}\right|^2\left|\frac{Dj\Omega+1}{A(j\Omega)^4 + B(j\Omega)^3 + C(j\Omega)^2 + Dj\Omega + 1}\right|^2 d\Omega \tag{7}$$

After the powers of the prediction residue have been calculated for the different components of the acceleration (i.e., P_{PEx}, P_{PEy}, and P_{Pez}), the average value (i.e., the average of the contributions of all the acceleration components) can be determined as

$$P_{PE} = \overline{P_{PEx} + P_{PEy} + P_{PEz}} \tag{8}$$

Equation (8) represents the road-surface roughness. The roughness index is obtained by applying a 10th-order moving average to P_{PE}.

When setting up the mobile application, the user configures the vehicle type (e.g., motorcycle, car, or truck) and mounting position (e.g., non-slip pad on the dashboard, dashboard phone mount, or pocket/other). Additionally, an accelerometric sensor calibration procedure is applied by keeping the smartphone in the hand as firmly as possible.

The issue of the orientation of the devices inside the vehicles can be looked at from two different approaches [36,37]. The first approach involves the preprocessing of the collected data, which aims to reorient the sensor data values from a device coordinate system to a local-level

Table 1
Excerpt from a SmartRoadSense dataset.

	Latitude	Longitude	P_{PE}	Osm_ID	Highway	Updated_at
1	45.47775	9.631453	0.05414	1.25E + 08	Primary	2015–11-14 18:02:23.310118
2	37.79954	12.42993	0.04048	71,174,815	Unclassified	2015–05-29 00:04:04.397805
3	45.47773	9.6312	0.0498	1.25E + 08	Primary	2015–11-14 18:02:23.310118
…	…	…	…	…	…	…
1,048,574	40.43489	16.83697	0.050205	2.34E + 08	Tertiary	2015–08-06 18:08:55.344815
1,048,575	40.43473	16.83683	0.04755	2.34E + 08	Tertiary	2015–08-06 18:08:55.344815
1,048,576	40.43454	16.83673	0.04124	2.34E + 08	Tertiary	2015–08-06 18:08:55.344815
…	…	…	…	…	…	…

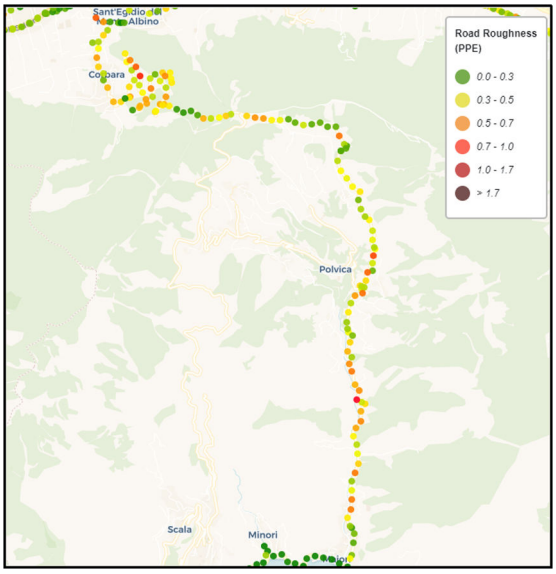

Fig. 2. SP2 quality map obtained from SmartRoadSense.

coordinate system using Euler angles. The second approach involves an orientation-independent featured, because the magnitude of the sensor data values on all three axes (see Eq. (8)) is considered instead of their individual values on three separate axes. It must also be noted that the mounting position of the device (non-slip pad on the dashboard, dashboard phone mount, or pocket/other) affects the detection rates performance [14,38,39].

The SmartRoadSense mobile application accesses the user's geographical location by GPS. It uses the device accelerometer to estimate the vehicle's acceleration. Recorded data are timestamped, and the model name, manufacturer name, and other general technical metadata are provided by the device. Data are processed on the device before transmission of coarse data. Unique identifiers of recording sessions and other sensitive data are never transmitted to the online service, but are kept on the device. All data collected by SmartRoadSense are released in an aggregate form as open data under the Open Database License (http://opendatacommons.org/licenses/odbl/1.0/). The road-surface irregularity data are provided as data points. Each roughness value represents a 20-m section of the road and is the average of all observations from users of that section. In addition to the information on the degree of roughness, each row of the dataset contains geographic and accessory information. The columns of the table represent the following:

- *Latitude*: The WGS84 latitude coordinate at the middle of the section corresponding to the measured roughness.
- *Longitude*: The WGS84 longitude coordinate at the middle of the section corresponding to the measured roughness.
- P_{PE}: The average roughness value of the road section.
- *Osm_ID*: Road identification.
- *Highway*: Road category.
- *Updated_at*: Time of the latest update.

The aggregation process is performed every 6 hrs by means of all new individual user contributions. The main effect of crowdsourcing is that the aggregated roughness data points are computed considering contributions from all.

We used the dataset available online on April 29, 2019, in the form of an open_data.csv file consisting of 3,198,743 records (see Table 1). Fig. 2 shows a map of the aggregated road-quality measures on SP2, with P_{PE} divided into six levels (0.0–0.3, 0.3–0.5, 0.5–0.7, 0.7–1.0, 1.0–1.7, and > 1.7), where 0.0–0.3 indicates good quality, and > 0.7 indicates the presence of potholes and deep distresses. © SmartRoadSense. © OpenStreetMap.

2.2. Data collection and distress Cadastre of Province of Salerno data

Data were collected by the Traffic and Transport Office's technicians of the Province of Salerno through *in situ* surveys. The technicians particularly focused on the following five types of road distresses.

2.2.1. Potholes

These are circular holes that may reach the deepest layers of the pavement. They often originate from crocodile skin-cracks, general cracks, or pavement breakthroughs that result in break ups and material removal (Fig. 3a). The classification of their geometric characteristics is based on thickness ($t \leq 3$ cm or $t > 3$ cm) and width/length ($e < 20$ cm, 20 cm $\leq e \leq 40$ cm, or e > 40 cm).

2.2.2. Raveling/slippage cracking with detachment

This involves detachment of the wearing course from the underlying layers with the surface of the bottom layer clearly visible. The detachment involves only the wearing layer (Fig. 3b). The classification of the geometric characteristics is based on the thickness ($t \leq 3$ cm or $t > 3$ cm) and width/length ($e < 1.5$ m, 1.5 m $\leq e \leq 3.0$ m, or $e > 3.0$ m).

2.2.3. Depressions

These are depressions of irregular or elliptical shape with extensions of a few meters to>20 m. There is possible cracking of the boundary areas (Fig. 3c). The classification of the geometric characteristics is based on the thickness (e.g., skin-deep or deep) and width/length ($e <$ 1.5 m, 1.5 m $\leq e \leq 3.0$ m, or $e > 3.0$ m).

2.2.4. Distresses caused by local underground utilities

Hollows may appear because of improper installation of local underground utilities, possibly with cracks on their edges (Fig. 3d). The classification of the geometric characteristics is based on the thickness ($t \leq 3$ cm or $t > 3$ cm) and width/length ($e < 20$ cm, 20 cm $\leq e \leq 40$ cm, $e > 40$ cm).

2.2.5. Rutting/distress caused by linear underground utilities

This is caused by the strain of the superstructure on the vehicle wheels, with lateral reflux of the pavement material. The depth of strain extends to the bituminous conglomerate layers or deeper to the foundation and the subgrade (Fig. 3e). Hollows may appear because of

Fig. 3. Types of road distresses: a) pothole, b) raveling, c) depression, d) distress caused by local utility, e) rutting, and f) distress caused by linear utility.

improper restoration after the installation or repair of linear underground utilities, possibly with cracks on their edges (Fig. 3f). The classification of the geometric characteristics is based on the thickness ($t \leq 3$ cm, $t > 3$ cm) and width/length ($e < 5$ m, 5 m $\leq e \leq 20$ m, or $e > 20$ m).

The acquired data are recorded on survey sheets (Fig. 4) with the following weights assigned to the thickness and extension of the distress:

- $\text{weight}_{\text{SKIN-DEEP THICKNESS}} = 1$
- $\text{weight}_{\text{DEEP THICKNESS}} = 2$
- $\text{weight}_{\text{SMALL EXTENSION}} = 1$
- $\text{weight}_{\text{MEDIUM EXTENSION}} = 3$
- $\text{weight}_{\text{LARGE EXTENSION}} = 5$

The relative severity of each distress, S, is evaluated as $S = \text{weight}_{\text{thickness}} \times \text{weight}_{\text{extension}}$.

The relative severities are then categorized into three severity classes:

- $S \leq 2 \rightarrow$ low severity $= 5$;
- $S = 3 \rightarrow$ medium severity $= 10$;
- $S \geq 4 \rightarrow$ high severity $= 25$.

Fig. 5 shows the severity classification of the pothole-type distresses with varying thicknesses and extensions.

Relative weights are assigned based on the geometric characteristics of the road in the sections where the distresses are detected, as follows:

- Curved = 15;

DISTRESS

General Information
OBJECTID _____ *(automatically assigned)*
Road Name _____ *(to be edited and chosen from a list)*
Start Date _____
End Date _____
Validation End Date _____

CRITERIA	DESCRIPTION					RELATIVE WEIGHT	TOT MAX	MAX. WEIGHT	
TYPE	POTHOLE			☐				50	0–15 LOW criticality
	RAVELING/ SLIPPAGE CRACKING			☐					
	DEPRESSION			☐					
	LOCAL UNDERGROUND UTILITIES DISTRESS			☐					
	RUTTING/LINEAR UNDERGROUND UTILITIES DISTRESS			☐					
GEOMETRIC FEATURES	Thickness	*superficial*	SEE DETAILS in operating manual	☐	1	Low 5	25		16–30 MEDIUM criticality
		deep	SEE DETAILS in operating manual	☐	2	Medium 15			
	Width/Length	*small*	SEE DETAILS in operating manual	☐	1				
		medium	SEE DETAILS in operating manual	☐	3	High 25			31–50 HIGH criticality
		large	SEE DETAILS in operating manual	☐	5				
ROAD PROFILE	curved			☐		15	15		
	mixed			☐		10			
	straight			☐		5			
CIVIL ENGINEERING WORKS	Pothole corresponding to viaduct or tunnel			☐		10	10		

Fig. 4. Survey sheet for the Distress Cadastre of Province of Salerno.

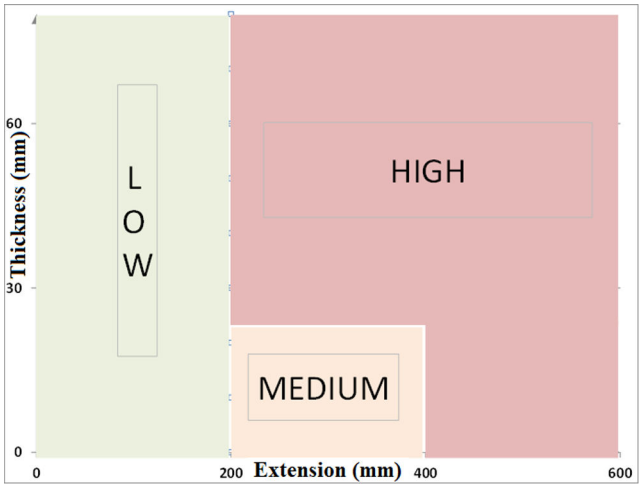

Fig. 5. Potholes severity classes.

- Mixed = 10;
- Straight = 5.

An additional relative weight is assigned for when the distress coincides with a major civil-engineering construction:

- Viaduct or tunnel = 10.

The total weight (TW) of a distress is within 0–50. Table 2 shows an excerpt from the dataset last updated on December 4, 2018, consisting of 201 georeferenced WGS84 records. Fig. 6 shows a map of the same data divided into three criticality classes (low: 0–15, medium: 16–30, and high 31–50).

2.3. Data collection and pavement condition index data

The PCI is used to quantify both the structural and functional characteristics of a surveyed pavement without directly measuring the structural capacity, roughness, or skid resistance. The acquisition of data on the various types of distresses enables timely identification of the main rehabilitation requirements and the development of an optimal maintenance process (Fig. 7).

The infrastructure is first divided into several utility branches, and each branch is then divided into sections based on the pavement design, maintenance history, and condition. The PCI procedure is well documented in the ASTM Standard [27]. In the present study, for road pavements having a bituminous conglomerate surface, we focus on all 20 possible types of distresses (see Table 3).

We inspected the study area between January 12 and April 24, 2019, measuring the observed distresses. We specifically considered the 6.5-m wide central strip of the road. 12 sections were identified and georeferenced at their start and end points (In Fig. 8, each point represents the end of a section and the start of the next). Each section of the considered strip was divided into 35-m long sample units, resulting in 23–82 sample units per section, 10–14 of which were inspected (Table 4).

Table 2
Excerpt from the Distress Cadastre of Province of Salerno dataset.

	Latitude	Longitude	OBJECTID	Road name	Frequency	Thickness	Extension	Road profile	Viaduct/tunnel	TW
1	40.717822°	14.613156°	5216	SP2a	medium distressed section	skin-deep	large	mixed	no	35
2	40.719925°	14.603620°	5218	SP2a	long distressed section	skin-deep	large	mixed	no	35
3	40.656813°	14.643025°	5219	SP2b	medium distressed section	skin-deep	large	mixed	no	35
…	…	…	…	…	…	…	…	…	…	…
199	40.669233°	14.643834°	56,824	SP2a	short distressed section	deep	medium	tangent	no	30
200	40.719548°	14.599333°	56,826	SP2a	short distressed section	skin-deep	small	mixed	no	15
201	40.702025°	14.646823°	56,833	SP2a	insulated	skin-deep	small	curved	no	20

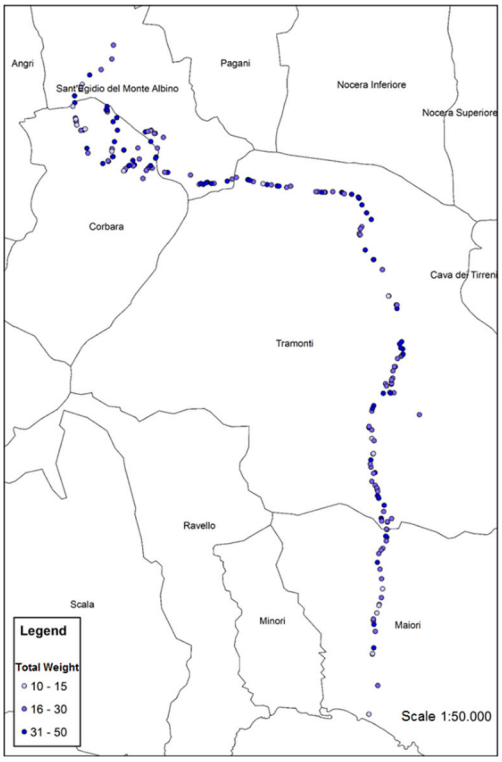

Fig. 6. SP2 quality map by the Cadastre of Province of Salerno.

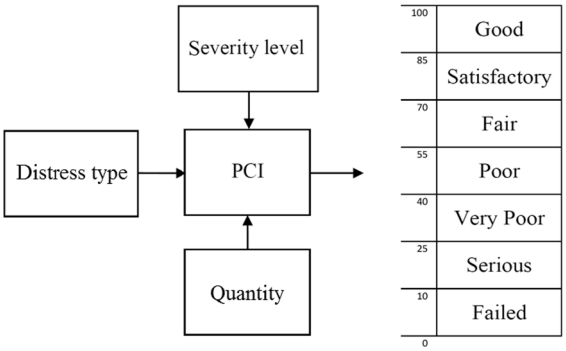

Fig. 7. PCI rating scale.

3. Data analysis

3.1. Comparison of SmartRoadSense and distress Cadastre of Province of Salerno data

The SmartRoadSense system performs continuous sampling along the entire stretch of road, with the sampling aggregated every 20 m. Conversely, the Distress Cadastre of Province of Salerno contains the points where operators find distresses. In total, 849 points were aggregated by SmartRoadSense along the SP2: one every 25.44 m on average. 201 distresses were recorded in the Cadastre by the operators: one every 107.5 m on average. To compare the SmartRoadSense data with that of the Distress Cadastre, we first matched the respective points at distances of ≤ 5 m, assuming that the points had a high probability of referring to the same distress. The maximum distance of 5 m takes into account the precision errors in the WGS84 coordinates, including the SmartRoadSense coordinates at which a vehicle senses the beginning of a distress (based on its front wheels) and the end of the distress (based on its rear wheels), and the Distress Cadastre coordinates at which an operator finds an extensive spatial distress. The threshold distance for attributing a pair of points to the same distress depends on many variables (e.g., different vehicles, GPS frequencies and accuracy). Owing to the probabilistic character of such an attribution, the authors proceeded to set a first-attempt threshold at 5 m. The following equation was used for the matching procedure, performed using geographical information or a common spreadsheet:

$$dist = \arccos(\cos(rad(90^{\circ} - lat1^{\circ})) \times \cos(rad(90^{\circ} - lat2^{\circ})) + sen(rad(90^{\circ} - lat1^{\circ}) \times sen(rad(90^{\circ} - lat2^{\circ})) \times \cos(rad(lon1^{\circ} - lon2^{\circ}))) \times 6,371 \times 1,000 \quad (9)$$

where *lat*1 is the latitude of the first point (dd), *lat*2 is the latitude of the second point (dd), *lon*1 is the longitude of the first point (dd), *lon*2 is the longitude of the second point (dd), and 6,371 is the average radius of the Earth in kilometers. The procedure returned 70 pairs of SmartRoadSense–Cadastre points, five of which are presented in Table 5. Fig. 9 shows a map of the same points along the SP2, where the blue and red points respectively correspond to SmartRoadSense and Distress Cadastre data. The degree of matching of the Cadastre points with those of the SmartRoadSense was 34.8% (70/201 = 0.348). Increasing the distance threshold beyond 5 m would lead to a matching degree of 100% (201/201 = 1) but with a lower probabilistic significance.

The six P_{PE} levels (0.0–0.3, 0.3–0.5, 0.5–0.7, 0.7–1.0, 1.0–1.7, >1.7) were regrouped into three classes (0.0–0.49, 0.50–0.99, and > 1.00) for comparison with the three criticality classes of Distress Cadastre (low: 0–15, medium 16–30, and high 31–50), as shown in the frequency histograms of Fig. 10.

Both histograms indicate lower frequencies in the low-criticality field and considerably higher frequencies in the medium- and high-criticality fields. The set of 70 pairs of matched points reflects a TW range for Distress Cadastre of $TW \in [\min_{TW} = 10, \max_{TW} = 40]$ and a P_{PE} range for SmartRoadSense of $P_{PE} \in [\min P_{PE} = 0.09366868, \max P_{PE} = 2.27316758]$. Because the scales of TW and P_{PE} differ, the values between their respective minima and maxima were normalized using Eq. (10):

$$var_{i,norm} = (var_i - min_{var})/(max_{var} - min_{var}) \quad (10)$$

The normalized values, ordered according to the direction of travel along SP2 (i.e., north to south), are plotted in Fig. 11.

On average, the P_{PEnorm} values were lower than the TW_{norm} values within their value ranges. This is reasonable, considering that

Table 3
Types of distresses in bituminous conglomerate pavements.

Types of pavement distress									
1	Alligator Cracking	2	Bleeding	3	Block Cracking	4	Bumps and sags	5	Corrugation
6	Depression	7	Edge cracking	8	Joint reflection cracking	9	Lane/shoulder drop-off	10	Longitudinal and transverse cracking
11	Patching and utility cut patching	12	Polished aggregate	13	Potholes	14	Railroad crossing	15	Rutting
16	Shoving	17	Slippage cracking	18	Swell	19	Raveling	20	Weathering

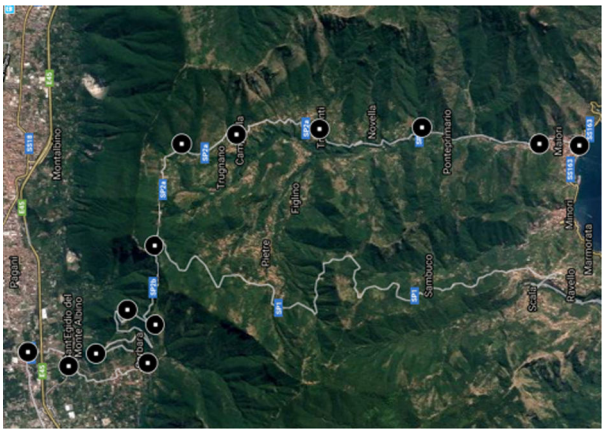

Fig. 8. Start and end points of the SP2 sections.

SmartRoadSense utilizes continuous detections along the entire road, whereas the points of Distress Cadastre are based on individually detected distresses. To evaluate the link between the two variables, $x = TW_{norm}$ and $y = P_{PEnorm}$, the Bravais–Pearson correlation index was estimated for the 70 pairs of points, $((x,y) = (TW_{norm},P_{PEnorm}))$, using Eq. (11):

$$r_{xy} = \frac{\sum_{i=1}^{n}(x_i - \bar{x})(y_i - \bar{y})}{\sqrt{\sum_{i=1}^{n}(x_i - \bar{x})^2 \sum_{i=1}^{n}(y_i - \bar{y})^2}} = 0.46379 \quad (11)$$

A moderate direct correlation was observed, indicating that the P_{PEnorm} values of SmartRoadSense increased with increasing TW_{norm} values of Distress Cadastre, and vice versa.

To investigate the influence of the distance threshold on the point matching, the TW and P_{PE} values can be weighted by their distance through multiplication by $1/\text{dist}_i$ (dist_i is given in the last column of Table 5). Thus, a greater weight is assigned to point pairs that are closer to each other. In fact, the aim is not to fix an optimal distance threshold, but to investigate the correlation between TW and PPE values. Fig. 12 shows the weighted and normalized variables, $TW_{w,norm}$ and $P_{PEw,norm}$:

Fig. 12 reveals the disposition of the $P_{PEw,norm}$ values, which can be observed to be very superimposable on the $TW_{w,norm}$ values. The Bravais–Pearson correlation index of the 70 point pairs $((x,y) = (TW_{w,norm}, P_{PEw,norm}))$, determined by Eq. (12), indicate a strong direct correlation:

$$r_{xy} = \frac{\sum_{i=1}^{n}(x_i - \bar{x})(y_i - \bar{y})}{\sqrt{\sum_{i=1}^{n}(x_i - \bar{x})^2 \sum_{i=1}^{n}(y_i - \bar{y})^2}} = 0.85306 \quad (12)$$

3.2. Comparison of SmartRoadSense and PCI data

Table 6 compares the PCI and average P_{PE} values for the 12 road

Table 4
SP2 Sections and sample units for PCI assessment.

Branch	Section	Lat_i Lat_f	Lon_i Lon_f	Length (m)	Considered central width (m)	Total sample units (n)	Surveyed sample units (n)	PCI sample units	PCI section
SP2b	1	40.739695 40.732893	14.596867 14.593756	1100	6.50	32	11	77, 69, 51, 80, 57, 59, 53, 70, 78, 59, 67	65
SP2b	2	40.732893 40.719796	14.593756 14.594530	2000	6.50	58	13	57, 51, 44, 62, 68, 55, 73, 59, 45, 70, 47, 50, 55	57
SP2b	3	40.719796 40.728347	14.594530 14.596525	1200	6.50	35	11	37, 53, 41, 34, 52, 29, 31, 29, 43, 37, 58	40
SP2b	4	40.728347 40.723159	14.596525 14.606220	2750	6.50	80	13	59, 41, 67, 47, 49, 45, 31, 37, 53, 41, 36, 43, 58	47
SP2b	5	40.723159 40.718507	14.606220 14.602880	1200	6.50	35	11	68, 62, 61, 73, 79, 66, 84, 70, 66, 81, 58	70
SP2b	6	40.718507 40.718581	14.602880 14.620187	1900	6.50	55	13	70, 81, 73, 59, 61, 57, 44, 49, 65, 56, 48, 60, 54	60
SP2a	7	40.718581 40.713917	14.620187 14.642621	2150	6.50	62	13	62, 58, 57, 68, 74, 62, 80, 66, 62, 76, 54, 75, 51	65
SP2a	8	40.713917 40.704722	14.642621 14.644602	1300	6.50	38	11	58, 64, 79, 56, 66, 60, 59, 71, 77, 64, 82	67
SP2a	9	40.704722 40.690958	14.644602 14.645862	2100	6.50	61	13	46, 49, 46, 59, 53, 72, 74, 57, 78, 63, 65, 61, 53	60
SP2a	10	40.690958 40.673873	14.645862 14.646147	2850	6.50	82	14	15, 39, 36, 35, 41, 44, 38, 47, 40, 38, 46, 34, 23, 20	35
SP2a	11	40.673873 40.654349	14.646147 14.642616	2250	6.50	65	13	39, 47, 27, 28, 41, 37, 28, 30, 51, 55, 41, 45, 53	40
SP2a	12	40.654349 40.647766	14.642616 14.642140	800	6.50	23	10	58, 64, 79, 56, 66, 60, 59, 71, 77, 64, 82	51

Table 5
Excerpt from the matched SmartRoadSense–Distress Cadastre points.

Nord-Sud	objectid	latC_SA	lonC_SA	weight	latSRS	lonSRS	P_{PE}	dist (m)
…	…	…	…	…	…	…	…	…
32	5302	40.71692	14.63307	25	40.7169	14.63304	0.63881429	3.328
33	51,340	40.71685	14.63369	35	40.71681	14.63368	1.14764446	4.145
34	30,856	40.71685	14.63413	25	40.71684	14.63411	1.13441118	1.821
35	5239	40.71685	14.6343	35	40.71686	14.63433	0.87730219	2.973
36	51,375	40.71692	14.63563	30	40.71689	14.63562	0.61249943	2.823
…	…	…	…	…	…	…	…	…

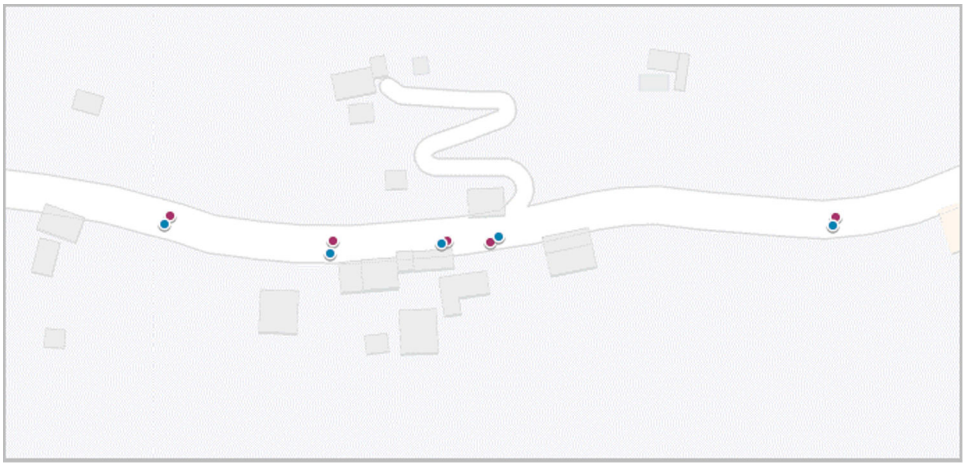

Fig. 9. Five matched SmartRoadSense (blue) and Distress Cadastre (red) points.

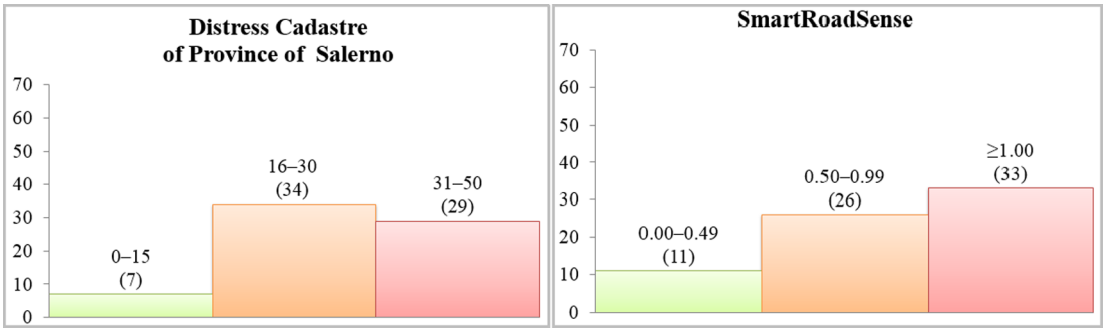

Fig. 10. Frequency histograms of the a) Distress Cadastre total weight and b) SmartRoadSense P_{PE}.

sections.

The normalized PCI and values are plotted in Fig. 13. It reveals trends in some opposite directions for PCI_{norm} and $_{norm}$. Application of the Bravais–Pearson correlation index to the 12 point pairs, $((x,y) = (PCI_{norm}, _{norm})$, produced r_{xy} = -0.34189, whose negative sign confirms an inverse correlation. This is expected, considering that the PCI increases with improving pavement conditions, whereas the decreases. The degree of correlation is moderate and is much lower than that obtained by the previous comparison of Cadastre and SmartRoadSense. This is be explained by the following:

- The PCI is representative of a road section and is calculated based on individual distresses, whereas the value for the section is obtained by aggregating the *Ppe* values for the different 20-m segments of the section. The coefficients of variation (see CV_{PCI} and CVcolumns in Table 6) indicate a higher degree of dispersion of the various P_{PE} values around , as well as a greater number of groupings of the PCI values.
- The surface distresses detected by SmartRoadSense are characterized by the acceleration of the vehicle wheels induced by the distress depth and transmitted to the mobile device inside the vehicle. However, among the 20 types of distresses, there are superficial ones (low-to-medium severity) that do not have an appreciable depth (e.g., alligator cracking, bleeding, block cracking, edge cracking, longitudinal and transverse cracking, polished aggregate, slippage cracking, raveling, and weathering).

4. Conclusions

The SmartRoadSense automatic and continuous road-monitoring system provides a regularly updated and detailed picture of the surface conditions of road pavements based on a roughness index directly determined from vehicles traveling the roads. The open availability of SmartRoadSense data, both in numerical and map formats, are significant resources for public managers of road infrastructures, offering an efficient and virtually cost-free means of monitoring the surface conditions of road networks for maintenance planning. This work contributes

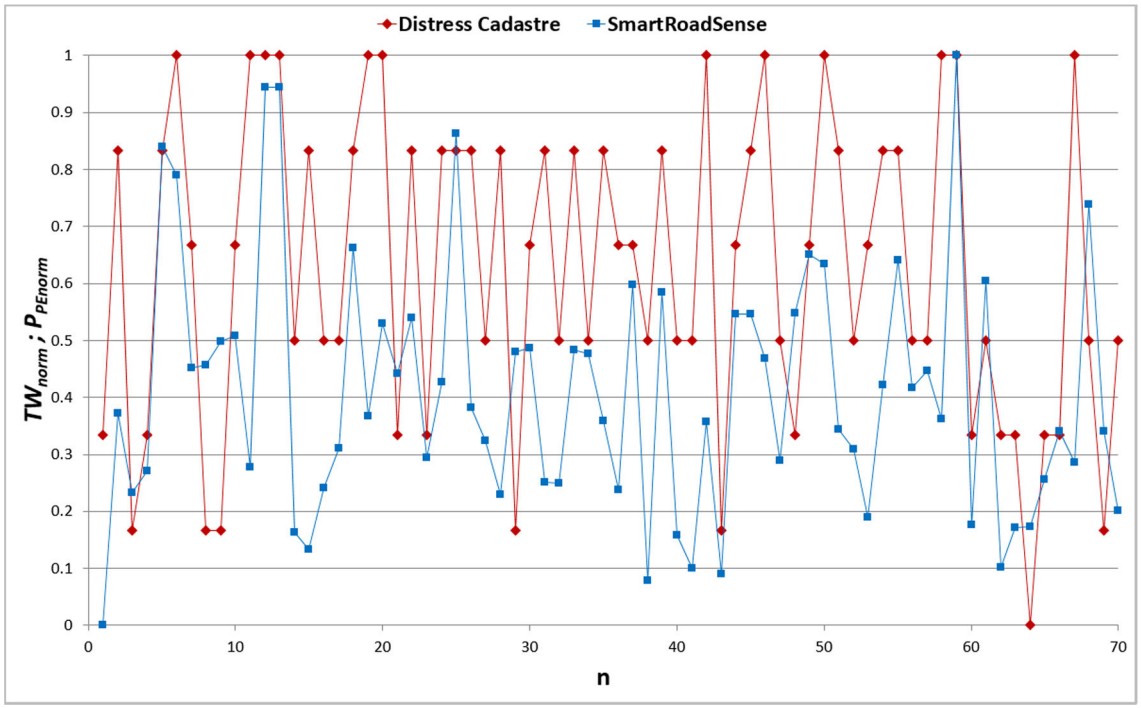

Fig. 11. Normalized values of *TW* (Distress Cadastre of Province of Salerno) and P_{PE} (SmartRoadSense).

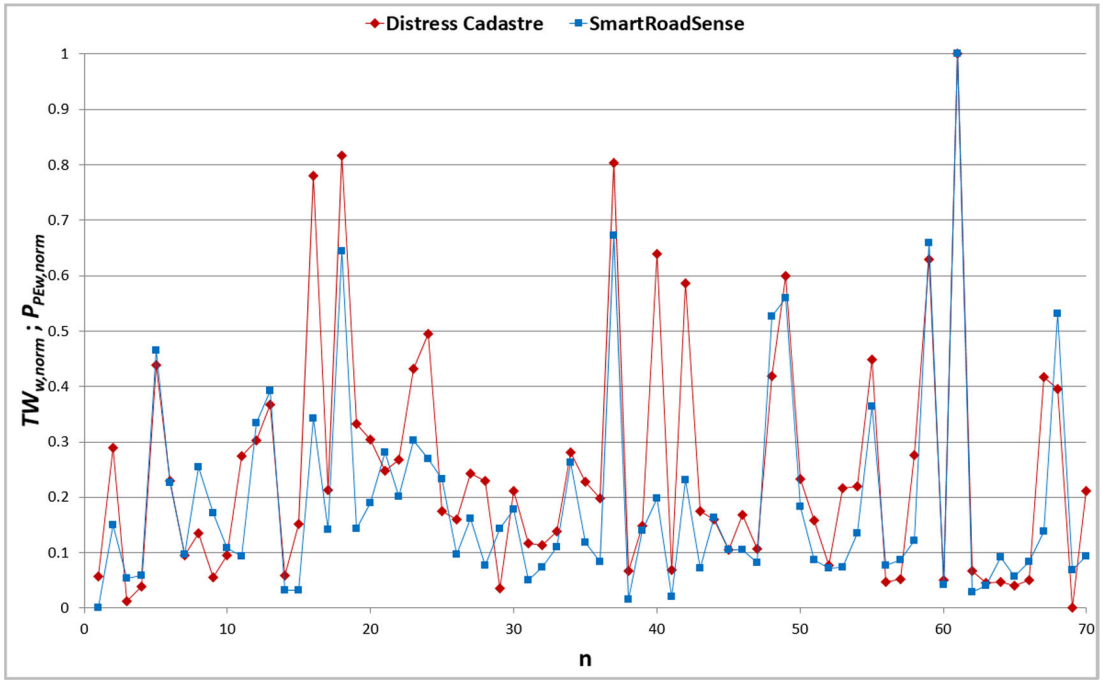

Fig. 12. Weighted and normalized *TW* and P_{PE}.

to the field by providing a comparative study of the results of crowd-sensing road-surface data and visual inspections. The study assessed whether any of the currently crowd-based monitoring technologies could be effectively used to replace visual road inspections. However, the comparison of this system with the two traditional road-survey methods showed that it was limited by an inability to specify the types of road distresses, because its data are based only on the dynamic parameter of acceleration. Thus, the distress must be of sufficient depth in order for the in-car mobile devices to capture appreciable acceleration metrics. Some types of low depth surface distresses, which also affect the safety and comfort of driving, may not be detected by the survey. Notably, when SmartRoadSense data are appropriately filtered, their indications are highly consistent with those of the Distress Cadastre of Province of Salerno [40], which focuses on five types of road distresses characterized by vertical thicknesses. However, the correlation is weaker when compared with PCI survey data, because nine of the 20 types of the low-to-medium distresses identified by the latter do not induce significant acceleration on vehicle wheels. Nevertheless, the

Table 6
Comparison of the PCI and values for the 12 road sections.

Section	PCI	$StDev_{PCI}$	CV_{PCI}		StDev	CV
1	65	10.27972	0.157051	0.2336752	0.15897	0.680306
2	57	9.48278	0.167495	0.5681803	0.23958	0.421657
3	40	10.11210	0.250525	0.6772121	0.21373	0.315599
4	47	10.29874	0.220566	0.5202586	0.24450	0.469962
5	70	8.55357	0.122512	0.5956024	0.19255	0.323281
6	60	10.48136	0.175364	0.4727818	0.27856	0.589187
7	65	9.10128	0.140020	0.5017948	0.23898	0.476258
8	67	9.04936	0.135249	0.5198649	0.27441	0.527850
9	60	10.48320	0.175621	0.4920706	0.19682	0.399989
10	35	9.64536	0.272248	0.5090123	0.19063	0.374504
11	40	9.82214	0.244613	0.7087259	0.20069	0.283164
12	51	8.37722	0.161722	0.2721858	0.11057	0.406221

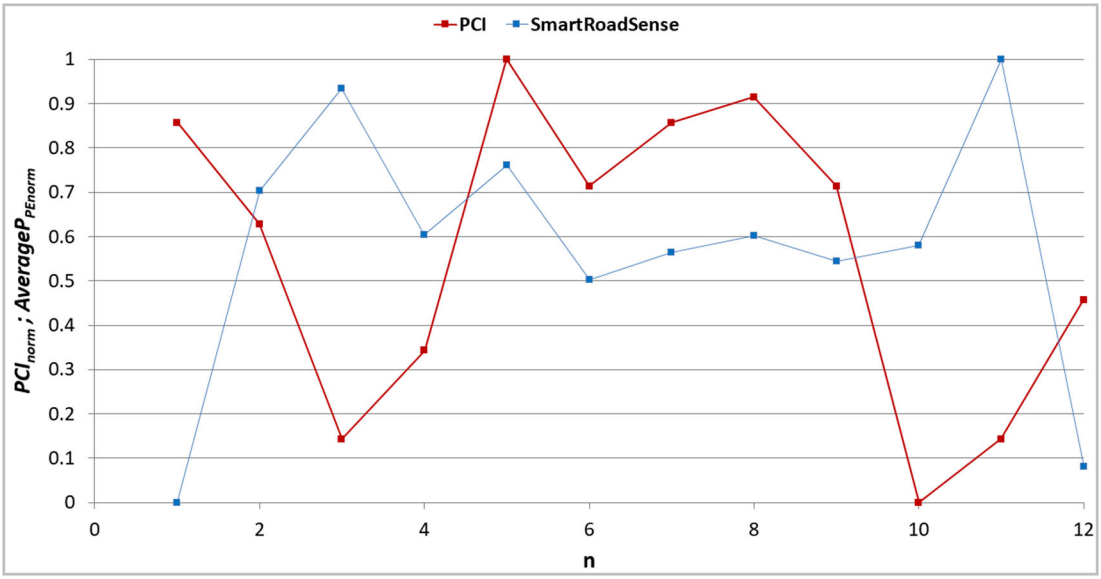

Fig. 13. Normalized PCI and values.

SmartRoadSense P_{PE} roughness index database is a significant resource for monitoring critical road failures (e.g., bumps, sags, corrugations, depressions, joint reflection cracks, lane or shoulder drop-offs, patches, utility-cut patches, potholes, railroad crossings, ruts, shoving, and swelling [27]) using acceleration metrics gathered by sensors in the vehicles, thus providing an indicative framework. However, for the purposes of effective maintenance, further analysis is required, including timely visual surveys that are more effective for identifying and classifying individual distresses. However, such an effort will be more cost intensive. Additionally, toward the development of a more robust automatic road-monitoring system that can identify all types of road-surface failures, the integration of dynamic systems, such as SmartRoadSense, with other technology, such as laser scanning, should be further explored.

5. Disclosure statement

The authors declare no conflict of interest.

6. Data availability

Some or all the data, models, and codes that support the findings of this study are available through the corresponding author upon reasonable request.

CRediT authorship contribution statement

Francesco Abbondati: Data curation, Methodology, Validation, Visualization, Writing - review & editing. **Salvatore Antonio Biancardo:** Methodology, Validation, Visualization, Writing - review & editing. **Rosa Veropalumbo:** Data curation, Validation, Writing - original draft. **Gianluca Dell'Acqua:** Conceptualization, Methodology, Supervision, Writing - original draft.

Declaration of Competing Interest

The authors declare that they have no known competing financial interests or personal relationships that could have appeared to influence the work reported in this paper.

Acknowledgements

The authors thank the staff of the Province of Salerno for providing information and sharing their insights into state-of-the-art practices in the measurement of road-surface distresses.

Funding sources.

This research did not receive any specific grant from any public, commercial, or not-for-profit funding agencies.

References

[1] C.H. Chin, S. Abdullah, S.S.K. Singh, A.K. Ariffin, D. Schramm, Durability assessment of suspension coil spring considering the multifractality of road excitations, Measurement 158 (2020), 107697, https://doi.org/10.1016/j.measurement.2020.107697.

[2] Society of Automotive Engineers, Ride and Vibration Data Manual: SAE J6A: Report of Riding Comfort Research Committee Approved July 1946 and Last Revised by the Vehicle Dynamics Committee October 1965, 1965.

[3] T. Dahlberg, Optimization criteria for vehicles travelling on a randomly profiled road–a survey, Vehicle Syst. Dyn. 8 (1979) 239–352, https://doi.org/10.1080/00423117908968607.

[4] Coopers and Lybrand, L.L.P., National Highway User Survey, National Quality Initiative Steering Committee, 1996.

[5] Y. Liu, Y. Wang, X. Cai, X. Hu, The detection effect of pavement 3D texture morphology using improved binocular reconstruction algorithm with laser line constraint, Measurement 157 (2020), 107638, https://doi.org/10.1016/j.measurement.2020.107638.

[6] K. Barri, B. Jahangiri, O. Davami, W.G. Buttlar, A.H. Alavi, Smartphone-based molecular sensing for advanced characterization of asphalt concrete materials, Measurement 151 (2020), 107212.

[7] J.Y. Wong, Theory of Ground Vehicles, John Wiley & Sons, 2001.

[8] T.D. Gillespie, Fundamentals of vehicle dynamics, Society of Automotive Engineers, 1992.

[9] K. Bogsjö, Road profile statistics relevant for vehicle fatigue, Ph.D. dissertation, Lund University, 2007.

[10] A. Gonzalez, E.J. O'brien, Y.-Y. Li, K. Cashell, The use of vehicle acceleration measurements to estimate road roughness, Vehicle Syst. Dyn. 46 (2008) 483–499. https://doi.org/10.1080/00423110701485050.

[11] J. Eriksson, L. Girod, B. Hull, R. Newton, S. Madden, H. Balakrishnan, The pothole patrol: using a mobile sensor network for road surface monitoring, Proceedings of the 6th International Conference on Mobile Systems, Applications, and Services, Breckenridge, CO, USA, June 2008, 29–39.

[12] P. Mohan, V.N. Padmanabhan, R. Ramjee, Nericell: rich monitoring of road and traffic conditions using mobile smartphones, Proceedings of the 6th ACM Conference on Embedded Network Sensor Systems, Raleigh, NC, USA, November 2008, 323–336.

[13] K. Chen, G. Tan, M. Lu, J. Wu, CRSM: A practical crowdsourcing-based road surface monitoring system, Wireless Netw. 22 (2016) 765–779, https://doi.org/10.1007/s11276-015-0996-y.

[14] C.-W. Yi, Y.-T. Chuang, C.-S. Nian, Toward crowdsourcing-based road pavement monitoring by mobile sensing technologies, IEEE Trans. Intell. Transport. Syst. 16 (2015) 1905–1917, https://doi.org/10.1109/TITS.2014.2378511.

[15] G. Alessandroni, A. Bogliolo, Carini, S. Delpriori, V. Freschi, L. Klopfenstein, E. Lattanzi, G. Luchetti, B. Paolini, A. Seraghiti, Demo: Mobile crowdsensing of road surface roughness, Proceedings of the 13th Annual International Conference on Mobile Systems, Applications, and Services, May 2015, 439.

[16] A. Bogliolo, A. Aldini, G. Alessandroni, A. Carini, S. Delpriori, V. Freschi, L.C. Klopfenstein, E. Lattanzi, G. Luchetti, B.D. Paolini, A, Seraghiti, The SmartRoadSense website, University of Urbino, http://smartroadsense.it/, 2015 (accessed [28 July 2020]).

[17] G. Alessandroni, A. Carini, E. Lattanzi, A. Bogliolo, Study on the influence of speed on road roughness sensing: the SmartRoadSense case, Sensors 17 (2017) 305, https://doi.org/10.3390/s17020305.

[18] G. Alessandroni, L. Klopfenstein, S. Delpriori, M. Dromedari, G. Luchetti, B. Paolini, A. Seraghiti, E. Lattanzi, V. Freschi, A. Carini, A. Bogliolo, Smartroadsense: collaborative road surface condition monitoring, Proceedings of the UBICOMM 2014: The Eighth International Conference on Mobile Ubiquitous Computing, Systems, Services and Technologies, Rome, Italy, 2014, 210–215.

[19] V. Freschi, S. Delpriori, L.C. Klopfenstein, E. Lattanzi, G. Luchetti, A. Bogliolo, Geospatial data aggregation and reduction in vehicular sensing applications: the case of road surface monitoring, Proceedings of the 3rd International Conference on Connected Vehicles & Expo, 2014. https://doi.org/10.1109/ICCVE.2014.7297643.

[20] H. Bello-Salau, A.M. Aibinu, E.N. Onwuka, J.J. Dukiya, M.E. Bima, A.J. Onumanyi, T.A. Folorunso, A new measure for analysing accelerometer data towards developing efficient road defect profiling systems, J. Sci. Res. Rep. 7 (2015) 108–116, https://doi.org/10.9734/JSRR/2015/16840.

[21] G. Reina, A. Leanza, A. Milella, A. Messina, Mind the ground: a power spectral density-based estimator for all-terrain rovers, Measurement 151 (2020), 107136, https://doi.org/10.1016/j.measurement.2019.107136.

[22] US Army Corps of Engineers, PAVER Asphalt Distress Manual, US Army Construction Engineering Laboratories, TR 97/104, June 1997.

[23] US Army Corps of Engineers, PAVER Concrete Distress Manual, US Army Construction Engineering Laboratories, TR 97/105, June 1997.

[24] E.A. Sharaf, E. Reichelt, M.Y. Shahin, K.C. Sinha, Development of a methodology to estimate pavement maintenance and repair costs for different ranges of pavement condition index, Trans. Res. Rec. 1123 (1987) 30–39.

[25] H. Shahnazari, M.A. Tutunchian, M. Mashayekhi, A.A. Amini, Application of soft computing for prediction of pavement condition index, J. Trans. Eng. 138 (2012) 1495–1506, https://doi.org/10.1061/(ASCE)TE.1943-5436.0000454.

[26] Y.U. Shah, S.S. Jain, D. Tiwari, M.K. Jain, Development of overall pavement condition index for urban road network, Procedia Soc. Behav. Sci. 104 (2013) 332–341, https://doi.org/10.1016/j.sbspro.2013.11.126.

[27] Standard practice for roads and parking lots pavement condition index surveys, American Society for Testing and Materials, 2011.

[28] R.M. Chalasani, Ride performance potential of active suspension systems–part I: Simplified analysis based on a quarter-car model, Proceedings of the 1986 ASME Winter Annual Meeting (1986).

[29] R.N. Jazar, Vehicle Dynamics: Theory and Application, Springer, 2008.

[30] B.R. Davis, A.G., Thompson, Optimal linear active suspensions with integral constraint, Vehicle Syst. Dyn. 17 (1988) 193–210. https://doi.org/10.1080/00423118808968911.

[31] T. Butsuen, The design of semi–active suspensions for automotive vehicles, Ph.D. dissertation, Massachusetts Institute of Technology, 1989.

[32] I. Fialho, G.J. Balas, Road adaptive active suspension design using linear parameter–varying gain-scheduling, IEEE Trans. Control Syst. Technol. 10 (2002) 43–54, https://doi.org/10.1109/87.974337.

[33] G. Verros, S. Natsiavas, C. Papadimitriou, Design optimization of quarter–car models with passive and semi–active suspensions under random road excitation, J. Vib. Control 11 (2005) 581–606, https://doi.org/10.1177/1077546305052315.

[34] J.T. Allison, Optimal partitioning and coordination decisions in decomposition-based design optimization, Ph.D. dissertation, The University of Michigan 131, 2008. https://doi.org/10.1115/1.3178729.

[35] M.M.M. Salem, A.A. Aly, Fuzzy control of a quarter–car suspension system, World Acad. Sci. Eng. Technol. 53 (2009) 258–263.

[36] S. Sattar, S. Li, M. Chapman, Road surface monitoring using smartphone sensors: s review, Sensors 18 (11) (2018) 3845.

[37] S. Sattar, Crowdsourcing Technique for Road Surface Monitoring using Smartphone Sensors, PhD Dissertation (2018).

[38] M. Jain, A.P. Singh, S. Bali, S. Kaul, Speed-Breaker EarlyWarning System, Proceedings of the NSDR: 6th USENIX/ACM Workshop on Networked Systems for Developing Regions, Boston, MA, USA, 15 June 2012.

[39] V. Douangphachanh, H. Oneyama, Estimation of road roughness condition from smartphones under realistic settings, Proceedings of the 2013 13th International Conference on ITS Telecommunications (ITST), Tampere, Finland, 5–7 November 2013, 433–439.

[40] M. De Luca, R. Mauro, F. Russo, G. Dell'Acqua, Before-after freeway accident analysis using cluster algorithms, Procedia Soc. Behav. Sci. 20 (2011) 723–731, https://doi.org/10.1016/j.sbspro.2011.08.080.